J Struct Funct Genomics (2015) 16:25–41
DOI 10.1007/s10969-015-9193-6

A SelB/EF-Tu/aIF2γ-like protein from *Methanosarcina mazei* in the GTP-bound form binds cysteinyl-tRNA^{Cys}

Tatsuo Yanagisawa · Ryohei Ishii · Yasushi Hikida · Ryuya Fukunaga · Toru Sengoku · Shun-ichi Sekine · Shigeyuki Yokoyama

Received: 17 December 2013 / Accepted: 10 January 2015 / Published online: 25 January 2015

Abstract The putative translation elongation factor Mbar_A0971 from the methanogenic archaeon *Methanosarcina barkeri* was proposed to be the pyrrolysine-specific paralogue of EF-Tu ("EF-Pyl"). In the present study, the crystal structures of its homologue from *Methanosarcina mazei* (MM1309) were determined in the GMPPNP-bound, GDP-bound, and apo forms, by the single-wavelength anomalous dispersion phasing method. The three MM1309 structures are quite similar (r.m.s.d. < 0.1 Å). The three domains, corresponding to domains 1, 2, and 3 of EF-Tu/SelB/aIF2γ, are packed against one another to form a closed architecture. The MM1309 structures resemble those of bacterial/archaeal SelB, bacterial EF-Tu in the GTP-bound form, and archaeal initiation factor aIF2γ, in this order. The GMPPNP and GDP molecules are visible in their co-crystal structures. Isothermal titration calorimetry measurements of MM1309·GTP·Mg^{2+}, MM1309·GDP·Mg^{2+}, and MM1309·GMPPNP·Mg^{2+} provided dissociation constants of 0.43, 26.2, and 222.2 μM, respectively. Therefore, the affinities of MM1309 for GTP and GDP are similar to those of SelB rather than those of EF-Tu. Furthermore, the switch I and II regions of MM1309 are involved in domain–domain interactions, rather than nucleotide binding. The putative binding pocket for the aminoacyl moiety on MM1309 is too small to accommodate the pyrrolysyl moiety, based on a comparison of the present MM1309 structures with that of the EF-Tu·GMPPNP·aminoacyl-tRNA ternary complex. A hydrolysis protection assay revealed that MM1309 binds cysteinyl (Cys)-tRNA^{Cys} and protects the aminoacyl bond from non-enzymatic hydrolysis. Therefore, we propose that MM1309 functions as either a guardian protein that protects the Cys moiety from oxidation or an alternative translation factor for Cys-tRNA^{Cys}.

Keywords Crystal structure · Translation factor · GTP · tRNA

Abbreviations

EF-Tu	Translation elongation factor Tu
EF-Sec	The selenocysteine tRNA-specific elongation factor or SelB
a/eIF2γ	Archaeal/eukaryotic initiation factor 2 gamma
PylRS	Pyrrolysyl-tRNA synthetase
SAD	Single-wavelength anomalous dispersion
SeMet	Selenomethionine
GMPPNP	Guanosine 5′-(β,γ-imido)triphosphate
ITC	Isothermal titration calorimetry
r.m.s.d.	Root mean square deviation

T. Yanagisawa · R. Ishii · Y. Hikida · R. Fukunaga · T. Sengoku · S. Sekine · S. Yokoyama
RIKEN Systems and Structural Biology Center, 1-7-22 Suehiro-cho, Tsurumi, Yokohama 230-0045, Japan

T. Yanagisawa · Y. Hikida · T. Sengoku · S. Yokoyama
RIKEN Structural Biology Laboratory, 1-7-22 Suehiro-cho, Tsurumi, Yokohama 230-0045, Japan

R. Ishii · Y. Hikida · R. Fukunaga · T. Sengoku · S. Sekine · S. Yokoyama (✉)
Department of Biophysics and Biochemistry, Graduate School of Science, The University of Tokyo, 7-3-1 Hongo, Bunkyo-ku, Tokyo 113-0033, Japan
e-mail: yokoyama@riken.jp

Present Address:
R. Fukunaga
Department of Biochemistry, School of Medicine, Johns Hopkins University, 725 N. Wolfe Street, 521A Physiology Bldg., Baltimore, MD 21205, USA

S. Sekine
RIKEN Center for Life Science Technologies, 1-7-22 Suehiro-cho, Tsurumi, Yokohama 230-0045, Japan

Introduction

GTP-binding translation factors play important roles in the initiation, elongation, and termination steps of translation. Translation elongation factor Tu (EF-Tu) (EF1α in eukaryotes/archaea), a GTP-binding translation factor, forms a complex with an aminoacyl-tRNA (aa-tRNA) and delivers it to the A site of the translating ribosome [reviewed in 1–6]. EF-Tu binds all canonical aa-tRNAs with nearly the same affinity, when each tRNA is bound to its cognate amino acid [7]. After correct codon-anticodon pairing, EF-Tu hydrolyzes the GTP, and the resultant EF-Tu·GDP complex dissociates from the aa-tRNA and the ribosome [8]. Thus, EF-Tu is responsible for the correct selection and binding of the cognate aa-tRNA to the codon at the A site. The translation elongation cycle is dependent on the different conformations of EF-Tu·GTP and EF-Tu·GDP [9–11].

Homologues of EF-Tu are also involved in the initiation of translation and/or the elongation cycle for non-canonical amino acids. In archaea and eukaryotes, the initiator Met-$tRNA_i$ is delivered to the ribosome by initiation factor IF2. IF2 is a heterotrimeric complex in which the γ subunit, which is related to EF-Tu, binds GTP and Met-$tRNA_i$ [12–14]. Another EF-Tu homologue protein, SelB, works as a special elongation factor for selenocysteine incorporation [15–17]. Selenocysteine is genetically encoded by an internal UGA stop codon and the specific mRNA stem-loop structure, called SECIS (selenocysteine insertion sequence) [18]. In bacteria, GTP-bound SelB recognizes and binds a selenocysteine-specific tRNA. Via its C-terminal domain (domain IV), this ternary complex subsequently binds SECIS in the ribosome-bound mRNA, resulting in the translational incorporation of selenocysteine in response to the specific internal UGA codons [19]. In mammals, the SelB homologue EF-Sec lacks domain IV, and the adaptor protein SPB2 binds EF-Sec and recognizes the SECIS element [20, 21].

By analogy to selenocysteine incorporation, a similar mechanism was proposed for pyrrolysine incorporation into proteins. Pyrrolysine is the "22nd" translationally inserted amino acid encoded by the UAG codon, and was first found in the monomethylamine methyltransferase (*mtmB1* gene product) from *Methanosarcina barkeri* [22–24]. Pyrrolysine is directly ligated to $tRNA^{Pyl}$, bearing an anticodon complementary to the UAG codon, by pyrrolysyl-tRNA synthetase (PylRS) [25, 26]. In contrast to selenocysteine incorporation, the mechanism for the delivery of pyrrolysyl-$tRNA^{Pyl}$ to the ribosome, and the decoding of the internal UAG codon as pyrrolysine, remain unclear. It was previously proposed that a specific elongation factor, EF-Pyl, is involved in pyrrolysine incorporation [27, 28].

All three known *Methanosarcina* genomes encode a protein homologous to SelB, EF-Tu, and aIF2γ [accession codes: WP_011033255 (Q8PXB3), WP_011305992 (Q46DU9), WP_011024522 (Q8TH68)], while no selenocysteine-containing proteins are encoded. Therefore, this SelB/EF-Tu/aIF2γ homologue was a candidate for EF-Pyl. However, the SelB/EF-Tu/aIF2γ-like proteins are shorter than the bacterial SelB proteins, and lack domain IV of SelB. Furthermore, no cis-acting elements corresponding to SECIS are conserved or functionally important for the genes encoding pyrrolysine-containing proteins [29, 30].

Numerous structures of the EF-Tu/SelB/aIF2γ superfamily proteins have been solved, including the GMPPNP-bound, GDP-bound, and apo form structures of the EF-Tu proteins from *Thermus thermophilus* [31, 32], *Thermus aquaticus* [33], and *Escherichia coli* [34–36], the aSelB from *Methanococcus maripaludis* [17], and the aIF2γ proteins from *Pyrococcus abyssi* [37], *Methanocaldococcus jannaschii* [38], *Pyrococcus furiosus* [39], and *Sulfolobus solfataricus* [12–14, 40, 41].

EF-Tu consists of three distinct domains, referred to as domains 1, 2, and 3. Domain 1 (the G domain) is responsible for guanine nucleotide binding, while domain 2 participates in tRNA and aminoacyl binding. All of the EF-Tu homologue structures solved so far indicated that conformational changes occur upon GTP hydrolysis. In EF-Tu, the conformational changes involve a large domain movement, as well as the concerted motions of two regions, called switch I and switch II [35, 42, 43]. Between the GMPPNP-bound and GDP-bound forms, the relative orientation of domain 1 to domains 2/3 drastically differs, but that between domains 2 and 3 is identical. Unlike EF-Tu, the archaeal aSelB [17] and aIF2γ [12] both undergo significant conformational changes only in switches I and/or II, and the relative orientations of domains 1 and 2/3 are retained between the GDP- and GMPPNP-bound forms.

In the present study, we determined the crystal structures of one of the *Methanosarcina* SelB/EF-Tu/aIF2γ-like proteins, MM1309 from *M. mazei,* in the GMPPNP-bound, GDP-bound, and apo forms, and found that the three structures shared similar conformations. The aminoacyl-binding pocket of MM1309 was too small to accommodate the pyrrolysyl moiety, contrary to the previous hypothesis for pyrrolysine incorporation [27, 28]. Interestingly, we discovered that MM1309 binds cysteinyl (Cys)-$tRNA^{Cys}$, and slows its hydrolysis.

Results and discussion

MM1309 is a SelB/EF-Tu/aIF2γ-like protein

The *M. mazei* genome encodes the general archaeal elongation factor aEF1α (422 residues) and MM1309 (350

residues) (Fig. 1) [44]. The MM1309 homologues are strictly conserved among the methanogenic archaeal genera *Methanosarcina*, *Methanococcoides*, *Methanohalophilus*, *Methanolobus*, *Methanomethyloborans*, *Methanocella*, *Methanosaeta*, *Methanococcus*, and *Methanocaldococcus*. The sequence identities of *M. mazei* MM1309 with *M. maripaludis* aSelB and *E. coli* SelB are 28 and 25 %, respectively, while those with *T. aquaticus* EF-Tu and *P. abyssi* aIF2γ are 21 and 23 %, respectively. Actually, a previous phylogenetic analysis revealed that MM1309 resembles SelB, rather than EF-Tu (EF1α) and aIF2γ [45].

Overall structures of MM1309

We determined the crystal structures of *M. mazei* MM1309 in the GMPPNP-bound, GDP-bound, and apo forms at 1.7, 1.9, and 1.55-Å resolutions, respectively ("Materials and methods", Table 1). The asymmetric unit contains one MM1309 molecule, and its 350 residues and the 11 tag-derived residues are all visible in the electron density map (Figs. 1, 2). The models show good geometry and all residues are in the allowed regions of the Ramachandran plot, as evaluated by Procheck [46] and Molprobity [47]. No significant structural differences were observed between these three forms, except for the nucleotide bound to the protein, as discussed below. The r.m.s.d. values between the three structures are less than 0.1 Å for 350 Cα atoms (Fig. 3). Hence, for the structure analysis in this study, the coordinates of the apo form, with the best resolution, were used unless otherwise noted.

MM1309 consists of three structural domains (domains 1–3), a common feature in the members of the EF-Tu/SelB/aIF2γ superfamily (Figs. 1, 2). Domain 1 (residues 1–169) contains the nucleotide binding site, and consists of seven β strands surrounded by five α helices and one 3_{10} helix. Domain 2 (residues 170–257) and domain 3 (residues 258–350) are β barrel structures, consisting of nine and seven β strands, respectively. Domains 1 and 2 are connected with a long α helix (α5) in domain 1 and a short 3_{10} helix (η2) in domain 2. In contrast, domains 1 and 2 in the EF-Tu structure are connected by a loop, which corresponds to the hinge region for the large domain movement. MM1309 is in the closed domain conformation: domain 1 is packed onto domains 2 and 3, and adopts the same domain organization as that in the EF-Tu·GMPPNP complex (Figs. 2, 3a–c). The structure of the connecting region of MM1309 is much more rigid than that of EF-Tu, implying that the closed conformation is the most stable structure, and large domain movement upon nucleotide binding is unlikely. The closed domain arrangement has also been observed for SelB and aIF2γ (Fig. 3d) [12, 17]. A DALI search [http://www.ebi.ac.uk/dali, 48] revealed that the structure of *M. mazei* MM1309 superimposed well on those of *M. maripaludis* aSelB (PDB codes: 4ACA, 4ACB, and 4AC9) [17], *Aeropyrum pernix* aEF1α (PDB codes: 3WXM and 3VMF) [49, 50], *S. solfataricus* aIF2γ (PDB codes: 2AHO, 3PEN, and 4M53) [12], *T. thermophilus* EF-Tu (PDB codes: 1EXM, 4LC0, 4LBV, 4LBY, 4LBZ, 4LBW, and 4H9G) [51], and *T. aquaticus* EF-Tu (PDB codes: 1EFT, 1B23, and 1TTT) [10, 31, 33], with Z-scores of 36.0–37.8, 36.8–37.4, 35.9–36.5, 35.9–36.2, and 35.8–36.1, respectively. The r.m.s.d. values between MM1309 and the EF-Tu/SelB/aIF2γ superfamily proteins are as follows: *M. maripaludis* aSelB·GMPPNP (4ACB, 2.6 Å for 340 Cα atoms) [17], *T. aquaticus* EF-Tu·GMPPNP·Phe-tRNA^{Phe} (1TTT, 2.5 Å for 336 Cα atoms) [31], *T. thermophilus* EF-Tu·GMPPNP (1EXM, 2.5 Å for 336 Cα atoms), *E. coli* EF-Tu·GMPPNP (2BVN, 2.8 Å for 340 Cα atoms) [52], *A. pernix* aEF1α·GTP·Pelota (3WXM, 2.2 Å for 334 Cα atoms) [49], *P. abyssi* aIF2γ (1KK2, 2.7 Å for 325 Cα atoms) [37], *S. solfataricus* aIF2γ·GDP (4M53, 2.4 Å for 331 Cα atoms), and *M. jannaschii* aIF2γ (1S0U, 2.7 Å for 314 Cα atoms) [38]. Thus, the closed form of MM1309 is not due to the crystal packing, but is the intrinsic structure of the protein.

The guanine nucleotide binding site of MM1309

The guanine nucleotide binding site in MM1309 is superimposable on those of the EF-Tu/SelB/aIF2γ superfamily proteins (Fig. 4). The electron density is well defined for the phosphate moiety and the guanine base, but is weaker for the ribose than the other moieties of GMPPNP. In the crystal of the MM1309·GMPPNP complex, the phosphate moiety is recognized by residues Lys11–Ser16 (corresponding to the EF-Tu residues His22–Thr26), which correspond to part of the P-loop (Fig. 4a–d) [53–55]. However, the highly-conserved Lys residue in the P-loop (GxxxxGK[S/T] where x can be any amino acid residue) is substituted with Arg (Arg14) in MM1309 (Fig. 1). Furthermore, the highly-conserved catalytic His residue of the Pro-Gly-His sequence in the GTPase family [56] is replaced by Tyr50 in MM1309 (Fig. 1). The main-chain nitrogen atoms of Lys11, Ser12, Gly13, Thr15, and Ser16 interact with the phosphate moiety. In addition, the side chain of Ser15 hydrogen bonds with one of the phosphate oxygen atoms. The amino group and the N^{ϵ} atom of Arg14 hydrogen bond with the β- and γ-phosphate moieties, respectively (Fig. 4b, d). By contrast, in the case of the Ras-like GTPases, the side-chain amino group of the conserved Lys residue recognizes the β- and γ-phosphate moieties [55].

The guanine ring is mainly recognized by the conserved Asp103, located in the 3_{10} helix between β6 and α4 (Figs. 1, 4b). The side-chain carboxyl group of Asp103 hydrogen bonds with the N1- and N2-atoms of the guanine moiety. In addition, the main-chain nitrogen atoms of Thr136 and Arg101 hydrogen bond with the O6 of the

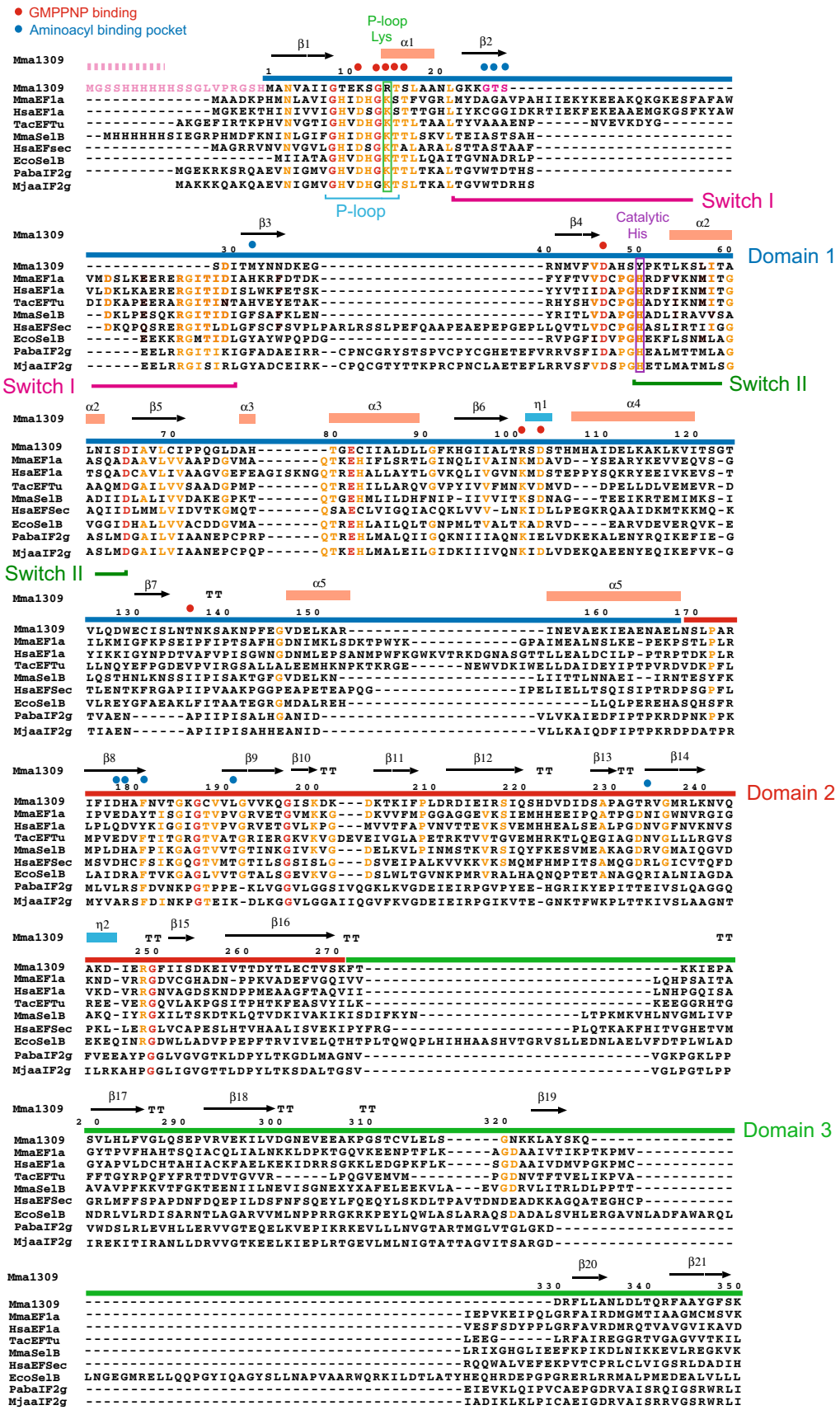
GMPPNP binding
Aminoacyl binding pocket
P-loop
Lys
Switch I
P-loop
Catalytic
His
Domain 1
Switch I
Switch II
Switch II
Domain 2
Domain 3
Mma1309
MmaEF1a
HsaEF1a
TacEFTu
MmaSelB
HsaEFSec
EcoSelB
PabaIF2g
MjaaIF2g

◀**Fig. 1** Structure-based sequence alignment of MM1309 with EF-Tu, EF1α, SelB, EF-Sec, and aIF2γ. The amino acid sequences were aligned using the programs CLUSTAL W [94] and ESPript [95], and then parts were optimized and adjusted manually. Completely and highly conserved amino acid residues are colored red and orange, respectively. The P-loop Lys residue, which interacts with the guanine nucleotide, and the catalytic His residue conserved among the GTPase family members are boxed in green and purple, respectively, on the sequence alignment. The secondary structures (α-helices, 3_{10}-helices, and β-sheets) of MM1309 are shown as *light orange boxes*, *sky blue boxes*, and *black arrows*, respectively, on the *top line*. The MM1309 residues Lys11, Gly13, Arg14, Thr15, Ser16, Asp46, Arg103, Asp105, and Thr136, which interact with GMPPNP, are highlighted with *red circles* above the sequence alignment. The MM1309 residues Gly25, Thr26, Ser27, Met32, Met178, His179, and Leu191, which form the aminoacyl binding pocket, are highlighted with *blue circles* above the sequence alignment. The residues Gly25, Thr26, and Ser27, which are specific to MM1309, are *colored pink*. *Dashes* represent breaks in the actual amino acid sequences of the respective proteins, to allow sequence alignment with MM1309. The *numbers* at the *top* correspond to the amino acid residues of *M. mazei* MM1309. The hexahistidine tag derived from pET28 is *colored light pink*, and the disordered region (residues Met-20–His-11) of MM1309 is shown with a *light pink dotted line* above the sequence alignment. The P-loop (Gly8–Thr15), switch I (Gly22–Ile30), and switch II (Tyr50–Asp65) regions are underlined in *sky blue*, *pink*, and *green* below the sequence alignment. Mma1309, *M. mazei* MM1309 (AAM31005); MmaEF1a, *M. mazei* aEF1α (AAM31960); HsaEF1a, *Homo sapiens* EF1α (ABO30531); TacEFTu, *T. aquaticus* EF-Tu (CAA46998); MmaSelB, *M. maripaludis* aSelB (CAF30892); HsaEFSec, *Homo sapiens* EF-Sec (NP_068756); EcoSelB, *E. coli* SelB (AAC76614); PabaIF2 g, *P. abyssi* aIF2γ (Q9V1G0); MjaaIF2 g, *M. jannaschii* aIF2γ (Q58657)

guanine moiety, directly and via a water molecule, respectively. The side-chain oxygen atom of Thr136 also interacts with the N7 atom of the guanine moiety, via a water molecule. There is no specific interaction between the ribose moiety and MM1309. This may be one of the reasons why the electron density is weaker for the ribose, as compared to those for the guanine and phosphate moieties. The Mg^{2+} ion is mainly coordinated by the β- and γ-phosphate moieties (3.0 Å) and a water molecule (2.3 Å) (Fig. 4b, d). In addition, the side chain atoms of Thr15 (2.9 Å), Arg14 (3.4 Å), and Asp46 (3.3 Å) participate in the Mg^{2+} coordination. The N^{ϵ} of Arg14 also interacts with the water molecule coordinating Mg^{2+}. In the MM1309·GDP structure, the Mg^{2+} is coordinated by the five atoms in the same manner, except for the γ-phosphate moiety (Fig. 4e).

In the apo-form structure, there are three water molecules corresponding to the phosphate oxygen atoms, which form a hydrogen bonding network (Fig. 4f). These water molecules hydrogen bond with the side-chain guanidino group of Arg14, the main-chain nitrogen atoms (Lys11, Ser12, Thr15, and Ser16), and the side-chain oxygen atoms (Ser12 and Ser16), mimicking the interactions between the phosphate moieties and MM1309 in the GMPPNP-bound form. Regarding the guanine-binding site, the N1 and O6 atoms are replaced by water molecules, which hydrogen bond with Asp103 and Thr136. As a result, the conformations of the nucleotide-binding sites are the same in the three structures.

The switch I and II motifs are involved in domain interactions, rather than nucleotide binding

In many GTPases with solved structures of the GTP (GMPPNP)-bound, GDP-bound, and/or apo forms, significant conformational changes occur only in two regions, called "switch I" and "switch II" (Figs. 2, 5) [35, 42, 43]. In general, these regions interact with the phosphate moieties, and undergo conformational changes in the GTP hydrolysis cycle. For example, the structure of SelB in the GDP-bound form is very similar to that of the apo form, and differs only in the switch II region [17]. In aIF2γ, the structural change is limited to the switch I and II regions, among the GTP (GMPPNP)-bound, GDP-bound, and apo forms [39]. In contrast, both regions in MM1309 are primarily involved in domain–domain interactions, rather than interactions with the phosphate moieties (Figs. 2, 3, 5).

In EF-Tu, switch I (Thr32–Thr65) is located near the GTP binding site. The residues Tyr47, Asp51, and Thr62 in the switch I region interact with the GMPPNP phosphate moieties and the Mg^{2+} ion (Fig. 5a). Furthermore, the main-chain nitrogen atom of Gly84 in switch II (His85–Asp100) hydrogen bonds with the γ-phosphate moiety of GMPPNP. The switch II region is located near domains 1 and 2, but there are no interactions between the switch I region and domains 2/3, except for the hydrogen bonding interactions between Gln98 and Glu226/Asn285. In MM1309, the region corresponding to switch I (Gly22–Ile30) forms a β strand (β2) and is located far from the nucleotide binding site (Fig. 5b). Moreover, the switch I region is involved in the interaction between domains 1 and 2. The side chain of Thr26 interacts with that of Arg234 in domain 2, via a water molecule. The side chain of Ser28 hydrogen bonds with those of His179 and Arg249 in domain 2. The side chain of Arg249 also interacts with that of Asp29. These interactions may stabilize the relative orientation of domains 1 and 2. There is no direct interaction between the switch II region and GTP. The side chain of Asp46 interacts with the Mg^{2+} ion (Fig. 5b). Furthermore, part of the switch II region (Tyr50–Asp65) interacts with domains 2 and 3. The main-chain carbonyl group of Asn62 hydrogen bonds with the side chain of Lys195, while the side-chain amide group of Asn62 hydrogen bonds with the main-chain carbonyl group of Gly287. The main-chain carbonyl group of Pro51 hydrogen bonds

Table 1 Data-collection and refinement statistics

	M.mazei MM1309 SeMet, GMPPNP-bound form	*M.mazei* MM1309 SeMet, GDP-bound form	*M.mazei* MM1309 Native, apo form
PDB code	3WNB	3WNC	3WND
X-ray source	PF	PF	SPring-8
	BL5A	BL5A	BL41XU
Wavelength	0.9794	0.9794	1.0000
Space group	*P*2(1)2(1)2	*P*2(1)2(1)2	*P*2(1)2(1)2
Cell dimensions			
a (Å)	62.06	62.02	61.87
b (Å)	108.70	108.70	108.61
c (Å)	58.32	58.39	58.62
α, β, γ (°)	90, 90, 90	90,90,90	90, 90, 90
Resolution (Å)	50–1.6 (1.97–1.6)	50–1.9 (1.93–1.9)	50–1.55 (1.58–1.55)
I/σ (I)	34.49	14.4	16.48
	(3.39)	(2.8)	(1.84)
Completeness (%)	100 (100)	99.0 (89.1)	98.1 (99.9)
No. reflections	52,887	31,405	57,020
Redundancy (%)	14.3	6.7	4.9
R_{sym} [a]	9.2 (80.9)	3.7 (51.3)	8.9 (75.1)
Refinement			
R_{work} [b]/R_{free} (%)[c]	18.9/23.3	17.2/21.7	17.3/20.9
Resolution (Å)	19.88–1.7	33.49–1.9	27.15–1.55
No. atoms			
Protein	2,765	2,765	2,815
Others	33	29	26
Water	400	389	307
No. reflections (work/test)	39,680/4,434	29,802/1,555	51,110/5,781
Average B-factors			
Protein	18.18	23.20	23.22
Ligands	44.72	59.25	64.20
Water	31.02	35.35	31.26
R.m.s deviations			
Bond length (Å)	0.008	0.009	0.015
Bond angles (°)	1.6	1.6	1.665
Ramachandran plot			
Most favored (%)	92.3	92.3	91.3
Allowed (%)	7.4	7.7	8.6
Disallowed (%)	0.3	0.0	0.0

The numbers in parentheses are for the last shell

[a] $R_{sym} = \Sigma|I_{avg} - Ii\cdot|/\Sigma Ii$

[b] $R_{work} = \Sigma|F_o - F_c|/\Sigma\ F_o$ for reflections of work set

[c] $R_{free} = \Sigma|F_o - F_c|/\Sigma\ F_o$ for reflections of test set [5–10 % of total reflections for *M.mazei* MM1309]

with the side chain of Arg342. Leu54 forms van der Waals interactions with Phe285, Leu337, Arg342, and Phe343 in domain 3.

MM1309 has higher affinity for GTP than GDP and GMPPNP

The GTP- and GDP-bound forms of the translational GTPases including EF-Tu and SelB, regulate translation initiation, elongation, and termination on the ribosome [57]. We examined the affinities of MM1309 for GTP, GDP, and GMPPNP in the presence of Mg^{2+} ions, and GTP in the absence of Mg^{2+} ions, by isothermal titration calorimetry (ITC) (Fig. 6). MM1309 bound GTP·Mg^{2+} with a dissociation constant (K_d) of 0.43 μM (Fig. 6a), while that for GTP without Mg^{2+} could not be determined (Fig. 6b). On the other hand, MM1309 bound GDP·Mg^{2+} weakly, with a dissociation constant (K_d) of 26.2 μM (Fig. 6c). In general, EF-Tu binds GDP much more strongly than GTP (K_d^{GTP}, 0.375 μM; K_d^{GDP}, 0.0013 μM) [58], while SelB binds GTP more strongly than GDP

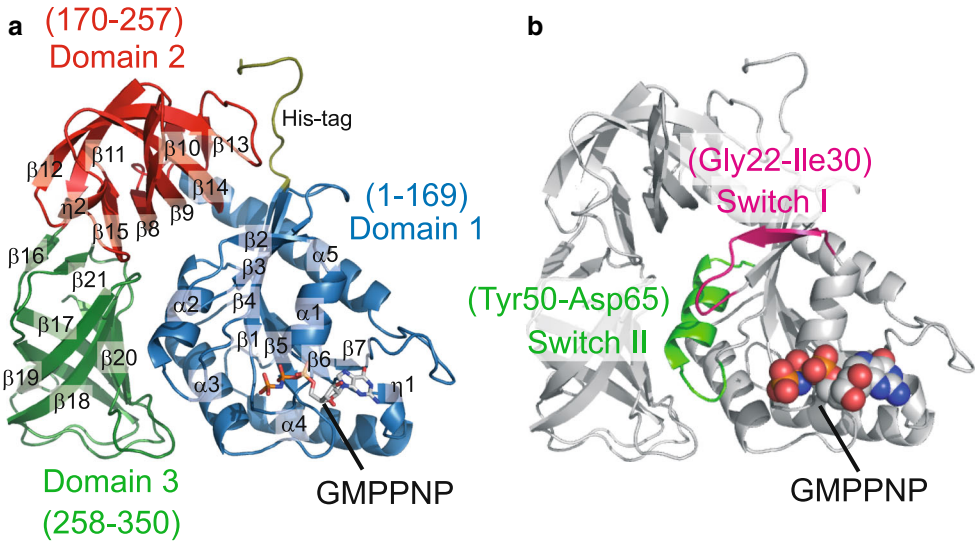

Fig. 2 Structure of MM1309 bound with a GTP analogue. **a** Ribbon diagrams of MM1309. The bound GTP analog (GMPPNP) is shown as a stick model. Domains 1, 2, and 3 of MM1309 are *colored blue*, *red*, and *green*, respectively. Secondary structure assignments (α-helices, 3_{10}-helices, and β-sheets) are shown as α, η, and β, respectively. **b** The switch I (Gly22–Ile30) and switch II (Tyr50–Asp65) motifs are *colored pink* and *green*, respectively. The GMPPNP molecule is shown as a space-filling model

(K_d^{GTP}, 0.7 μM; K_d^{GDP}, 13.4 μM) [59]. The K_d values of MM1309 for GTP and GDP are similar to those of SelB, rather than those of EF-Tu. These results indicated that, like SelB, MM1309 does not need a guanine nucleotide exchange factor (GEF). Surprisingly, MM1309 bound GMPPNP·Mg^{2+} much less strongly than GTP·Mg^{2+}, with a dissociation constant (K_d) of 222.2 μM (Fig. 6d). MM1309 did not hydrolyze GTP during the ITC analysis. We examined whether MM1309 has intrinsic GTPase activity in the absence of ribosomes by using radioactively-labeled [α-^{32}P]GTP and a fluorescent GTP analog, [2′-/3′-*O*-(*N*-methylanthraniloyl)guanosine-5′-*O*-triphosphate] (Mant-GTP), but did not detect any GTPase activity (data not shown). Therefore, MM1309 lacks GTPase activity, at least in the absence of ribosomes. These results are supported by the fact that the highly conserved P-loop Lys and catalytic His residues in the GTPase family are replaced by Arg14 and Tyr50, respectively, in MM1309 (Fig. 1).

Notably, the binding affinity of MM1309 for GMPPNP was 500 times lower than that for GTP (Fig. 6d). Therefore, the present GMPPNP-bound structure, which is very simlar to the GDP-bound structure, may be different from the true GTP-bound structure. In this context, the structural properties of the GTPase translation factors are diverse [60–80]. First, eukaryotic release factor 3 (eRF3) in complex with GMPPNP undergoes large conformational changes in the presence of eukaryotic release factor 1 (eRF1) and the ribosome [68–73], while eRF3 exhibits about 300 times lower affinity for GMPPNP than GTP in the presence of eRF1. In contrast, SelB displays similar affinities for GTP and GMPPNP, although its overall structures may differ between them [80]. However, EF-Tu undergoes large changes in the switch region conformations and the domain arrangement upon GMPPNP binding, whereas the conformation of elongation factor G (EF-G)·GMPPNP is the same as that of EF-G·GDP, but drastically changes upon ribosome binding [60–69]. Therefore, we should further investigate the true GTP-bound form and the GTPase activity of MM1309.

Docking models of MM1309 with aminoacyl-tRNAs

The structure of MM1309 superimposed well on those of the *T. aquaticus* EF-Tu·GMPPNP·Phe-tRNA^{Phe} (PDB code: 1TTT) and EF-Tu·GMPPNP·Cys-tRNA^{Cys} (PDB code: 1B23) ternary complexes (Figs. 3b, 7) [31, 33]. The 3′-end of the tRNA resides in a hydrophobic pocket composed of the side chains of Ile231, Val237, Leu289, and Glu271 in EF-Tu, which correspond to Val183, Val189, Arg238, and the Gln220 side chain in MM1309, respectively (Fig. 7a). However, the direction of the Gln220 side chain differs from that of Glu271 in the EF-Tu complex. Glu220 hydrogen bonds with the side chain of Ser218, which causes steric hindrance between MM1309 and the adenine base of the modeled tRNA (Fig. 7a). Therefore, Gln220 may undergo a conformational change upon tRNA binding, in order to accommodate A76 in the binding pocket. By contrast, the binding site for the 5′-end of the tRNA is blocked by the interdomain interaction, although the residues involved in the tRNA binding are well conserved between MM1309 and EF-Tu. In the EF-Tu ternary complex structure, Lys90 and Arg300, which respectively correspond to Lys55 and Arg249 in MM1309, are directly involved in the 5′ phosphate recognition (Fig. 7a). In MM1309, the aforementioned interdomain contacts may prevent the tRNA binding. Therefore, the residues should undergo conformational changes in order to interact with tRNA, which may rearrange the switch I and II conformations. A slight movement of the switch I region could be

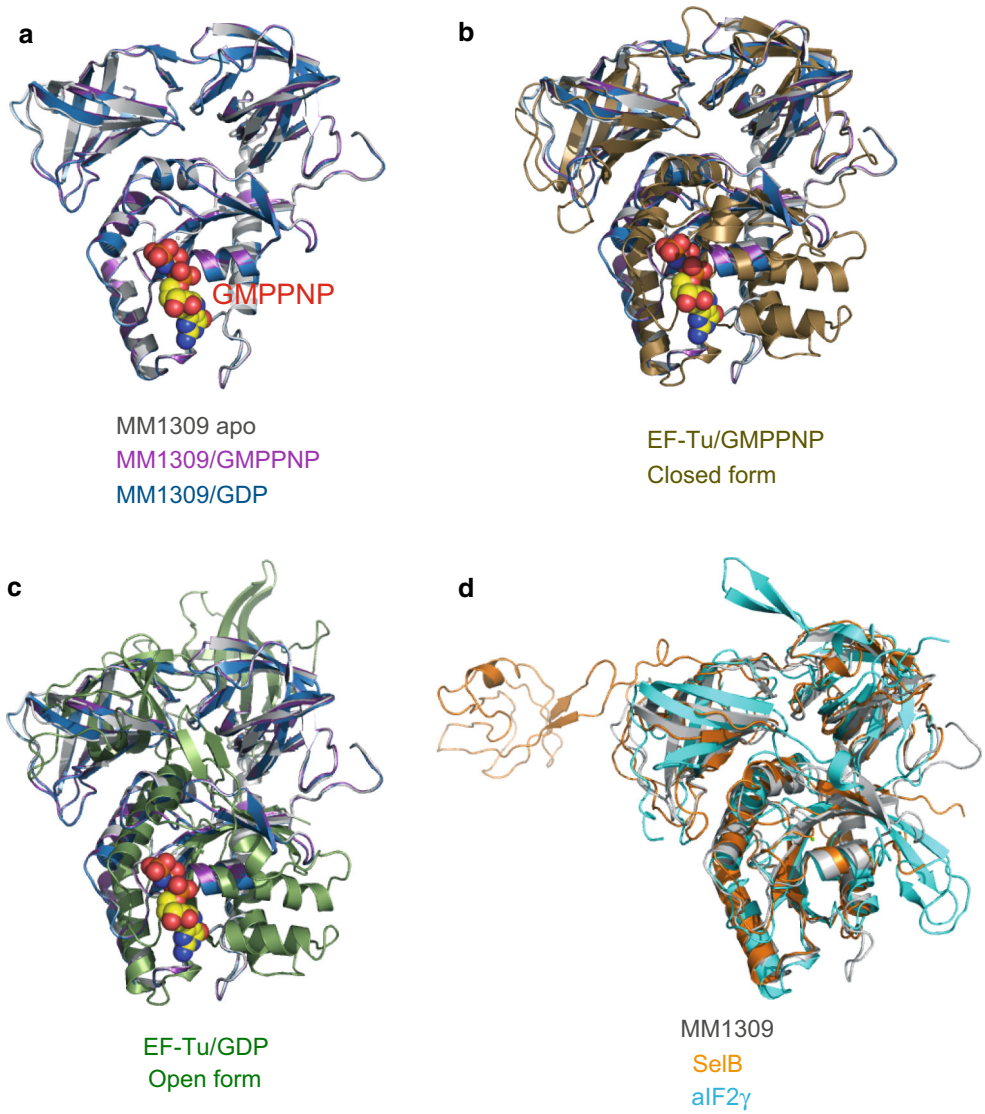

Fig. 3 Superposition of MM1309 with EF-Tu, aSelB, and aIF2γ, represented by ribbon models. **a** Superposition of the MM1309 structures in the GMPPNP-bound, GDP-bound, and apo forms. **b** Superposition of MM1309 with *T. aquaticus* EF-Tu in the GTP-bound form (PDB code: 1TTT). **c** Superposition of MM1309 with *T. aquaticus* EF-Tu in the GDP-bound form (PDB code: 1TUI). **d** Superposition of MM1309 with *M. maripaludis* aSelB (PDB code: 4ACA) and with *P. abyssi* aIF2γ (PDB code: 1KK0)

sufficient to accommodate the 5′-end of the tRNA, as judged by a comparison between the EF-Tu and MM1309 structures. The bottom of the aminoacyl binding pocket of EF-Tu, which is composed of His67, Glu226, Asp227, Phe229, Thr239, and Asn285, has sufficient space to accommodate the pyrrolysyl moiety (Fig. 7b). In contrast, the aminoacyl binding pocket of MM1309, which is composed of Gly25, Thr26, Ser27, Met32, His170, Asp178, Phe181, Leu191, and Arg234, is narrow and lacks space for the pyrrolysyl moiety (Fig. 7c). The MM1309 residues Gly25, Thr26, and Ser27 in β2, which are involved in the tRNA binding site, cause especially severe steric hindrance with the docked pyrrolysyl moiety (Fig. 7c).

The phylogenetic distributions of the MM1309 orthologues are different from those of the pyrrolysine, selenocysteine, and phosphoserine incorporation systems

A previous phylogenetic analysis revealed that the existence of the MM1309 proteins in archaea has no relevance to the presence of the pyrrolysine and selenocysteine incorporation systems [45]. Among archaea, a pyrrolysine-related protein (PylRS) exists only in *Methanosarcinaceae*. On the other hand, selenocysteine-related proteins (SelB and SelD) exist only in *Methanocaldococcaceae*, and *Methanococcaceae*, but not in *Methanosarcinaceae*, *Sulfolobaceae*, and

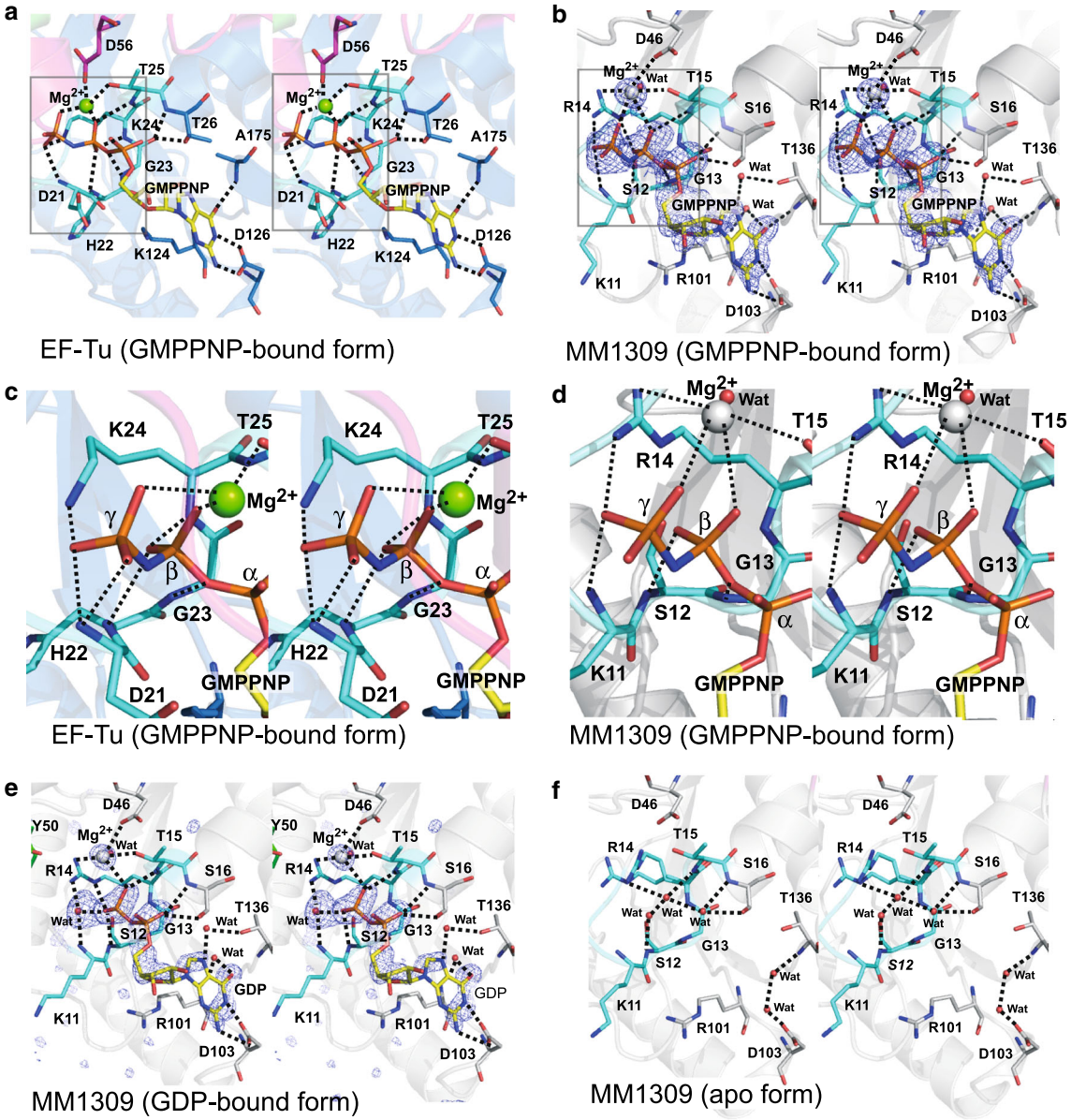

Fig. 4 Stereo views of the GTP binding sites. **a** The bound GMPPNP molecule in the *T. aquaticus* EF-Tu·GMPPNP·Mg^{2+} structure. **b** The bound GMPPNP molecule in the MM1309·GMPPNP·Mg^{2+} structure. The F_o–F_c omit map (contoured at 3.3 σ) of the bound GMPPNP·Mg^{2+} in the MM1309 active site. **c**, **d** Close-up stereo views around the γ-phosphate group of the bound GMPPNP in *T. aquaticus* EF-Tu·GMPPNP·Mg^{2+} (**c**) and MM1309·GMPPNP·Mg^{2+} (**d**). The amino acid residues surrounding the phosphate groups and the magnesium ions of the bound GMPPNP·Mg^{2+} are depicted by stick models. **e** The bound GDP molecule in the MM1309·GDP structure. The F_o–F_c omit map (contoured at 4.0 σ) of the bound GDP·Mg^{2+} in the MM1309 active site. **f** The GTP binding site in the MM1309 apo form. The MM1309 residues that are located close to the bound guanine nucleotide are represented as stick models. The P-loop motifs (Gly17–Thr25 in EF-Tu and Gly7–Thr15 in MM1309) are shown in *sky blue*. The switch I regions are *colored pink*. Transparent ribbon models of EF-Tu (*blue*) and MM1309 (*white*) are visible in the background

Thermoplasmataceae (Fig. 8). Furthermore, a phosphoserine-related protein [phosphoseryl-tRNA synthetase (SepRS)] exists in *Methanocaldococcaceae*, *Methanococcaceae*, *Methanosarcinaceae*, and *Archaeoglobaceae*, but not in *Sulfolobaceae* and *Thermoplasmataceae*, indicating that the phosphoserine system is also unrelated to the phylogenetic distribution of the MM1309 orthologues (Fig. 8). Regardless of the presence of the pyrrolysine, selenocysteine, and phosphoserine systems, the MM1309 genes might have been horizontally transferred among several archaea. Atkinson et al. [45] proposed that MM1309 binds Cys-RNA^{Cys} and protects the cysteinyl moiety from oxidation, after they examined the initial version of our MM1309 structure in the Protein Data Bank (PDB code: 2ELF) and considered that

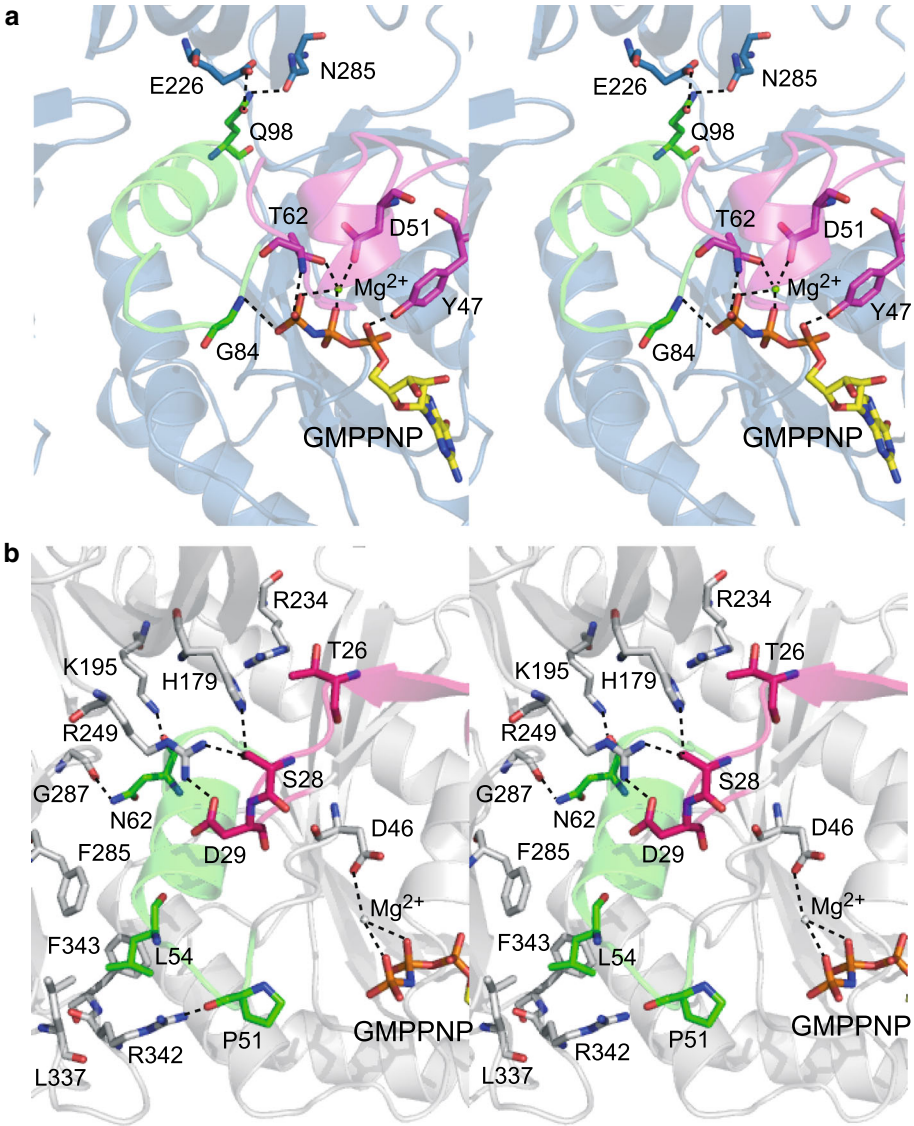

Fig. 5 Close-up stereo views of the switch I and II regions in EF-Tu (**a**) and MM1309 (**b**). The bound GMPPNP molecule and the Mg^{2+} ion, and the EF-Tu and MM1309 residues in the switch I and II regions, which are involved in the GMPPNP interactions, are shown as stick models. The EF-Tu and MM1309 residues that are involved in the domain–domain interactions are also shown as stick models. The switch I and II regions of MM1309 are involved in domain–domain interactions, rather than GTP/GDP interactions. The switch I and II regions are *colored pink* and *green*, respectively. Transparent ribbon models of EF-Tu (*blue*) and MM1309 (*white*) are visible in the background

MM1309 could accommodate the cysteinyl moiety in the aminoacyl binding pocket (Fig. 7c). Furthermore, the MM1309 proteins are conserved among anaerobic archaea. Anaerobic archaea might retain a similar strategy for cysteine protection, considering that the structural models for the aminoacyl sites of the MM1309 proteins from *S. solfataricus*, *M. jannaschii*, and *T. acidophilum* closely resemble that of MM1309 (data not shown).

MM1309 binds Cys-tRNA^{Cys}

Based on the hypothesis described above, we examined if MM1309 binds Cys-tRNA^{Cys} (Fig. 9). We prepared radioactively-labeled Cys-tRNA^{Cys} by using cysteinyl-tRNA synthetase (CysRS) and tRNA^{Cys} from *M. mazei* [81], and performed an aminoacyl-tRNA hydrolysis protection assay according to the standard method [82]. In the absence of MM1309, [^{14}C]Cys-tRNA^{Cys} was hydrolyzed with a half-life of 80 min (Fig. 9, blue line). On the other hand, the half-life of hydrolysis was much longer (300 min) in the presence of MM1309 (Fig. 9, green line), indicating that MM1309 binds Cys-tRNA^{Cys} and slows its hydrolysis.

What is the physiological role of MM1309 in *M. mazei* cells? As MM1309 homologues are conserved among many anaerobic archaea, it may be reasonable that MM1309 protects Cys-tRNA^{Cys} as a guardian in the oxidative environment. It is also possible that MM1309 acts as an alternative translation elongation factor, for the following two reasons. First, MM1309 might be able to accommodate the 20 canonical amino acids in the aminoacyl-binding pocket,

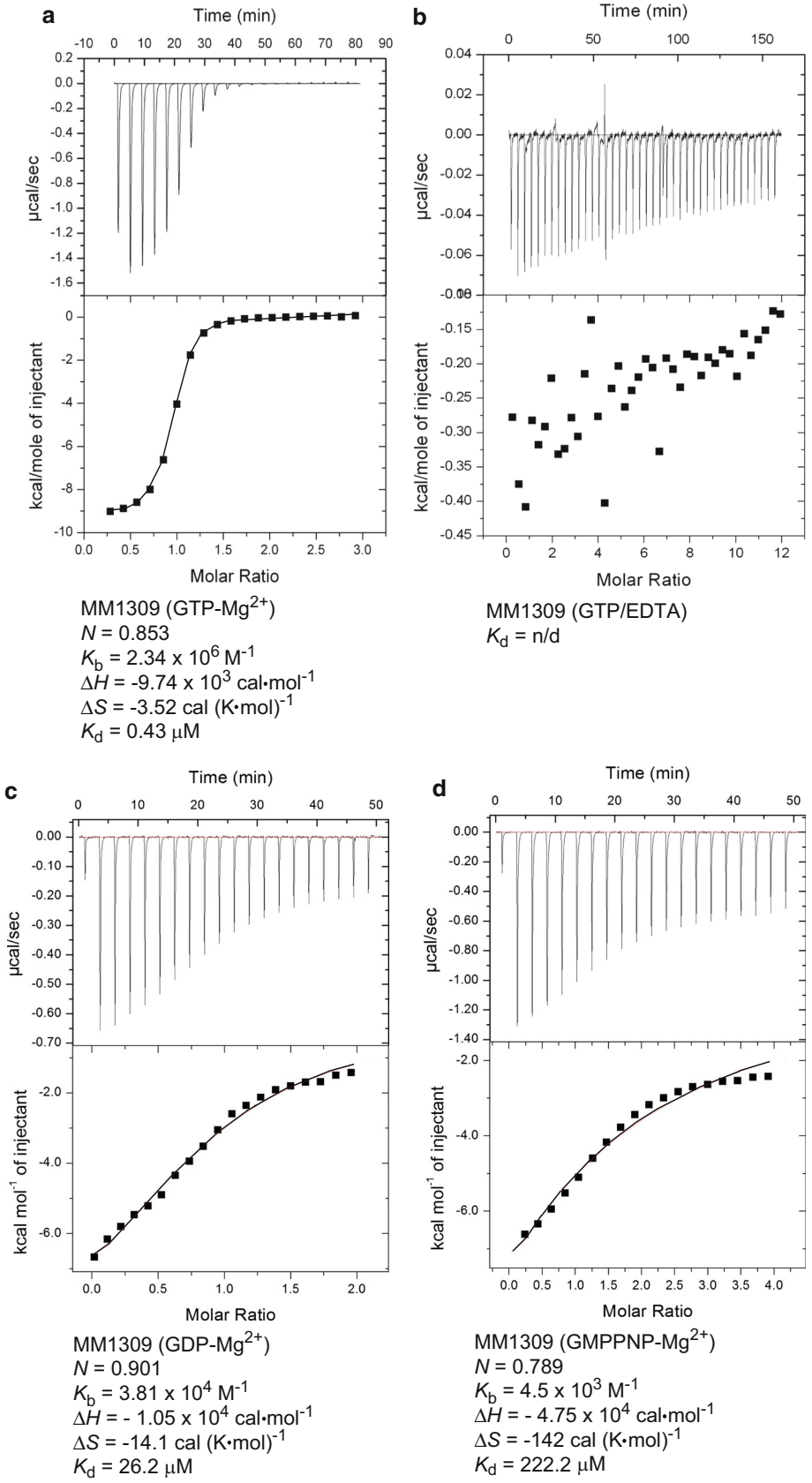

Fig. 6 ITC analysis. The upper and lower panels display the ITC titration curves and the binding isotherms, respectively, for MM1309 with GTP·Mg^{2+} (**a**), GTP without Mg^{2+} (**b**), GDP·Mg^{2+} (**c**), and GMPPNP·Mg^{2+} (**d**). *N*, the binding stoichiometry; K_b, the observed binding constant; K_d ($K_d = 1/K_b$), the dissociation constant; ΔH, the binding enthalpy; ΔS, the binding entropy

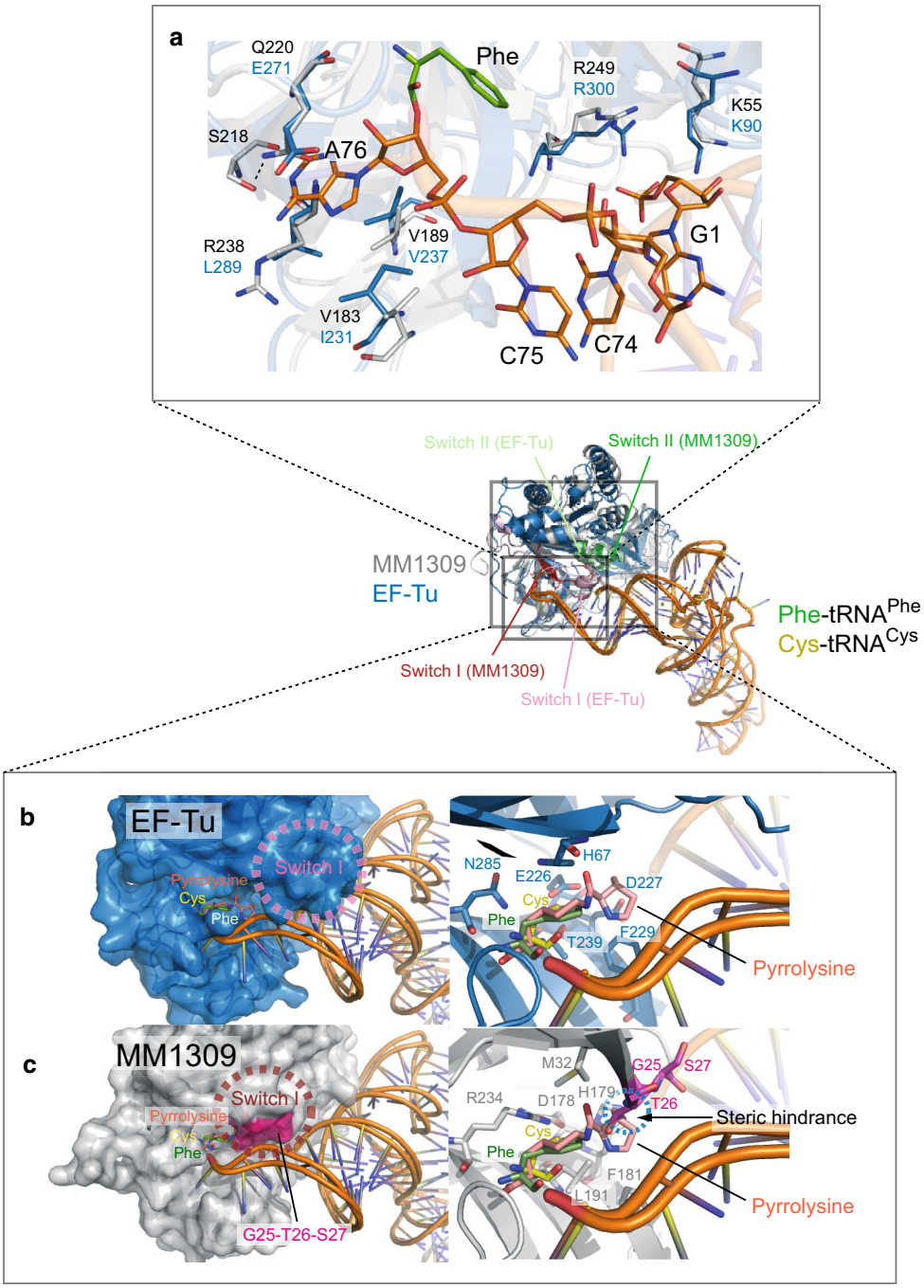

Fig. 7 Docking model of MM1309 with EF-Tu·Phe-tRNA^{Phe} and EF-Tu·Cys-tRNA^{Cys}. **a** Superimposition of the 5′-A and 3′-CCA tRNA binding site residues (shown as stick models) in MM1309 on those in EF-Tu·Phe-tRNA^{Phe}. **b**, **c** Comparison of the aminoacyl binding sites between MM1309 and EF-Tu. The MM1309 (*grey*) and EF-Tu (*marine blue*) residues superimposed well on each other. EF-Tu and MM1309 are represented as surface models, and tRNAs are represented as ribbon models. The modeled pyrrolysyl moiety is also shown as a stick model. In contrast to the aminoacyl binding pocket of EF-Tu, the MM1309 pocket lacks sufficient space to accommodate the pyrrolysyl moiety, because of the steric hindrance with Gly25, Thr26, and Ser27 in β2

based on the docking model. Second, *M. mazei* aEF1α, which contains 19 cysteine residues, might be prone to oxidation. On the other hand, MM1309 contains only 6 cysteine residues, and the purified protein remains soluble even under oxidative conditions. Thus, we propose the designation of MM1309, as well as its orthologues, as aEF-X, toward further investigations of the physiological roles of the aEF-X protein in *M. mazei* cells.

	MM1309 (a.a.)	aSelB (a.a.)	Pyrrolysine (PylRS)	Selenocysteine (SelD)	Phosphoserine (SepRS)
Crenarchaeota					
Sulfolobus solfataricus	+ (301)	−	−	−	−
Sulfolobus tokodaii	+ (286)	−	−	−	−
Euryarchaeota					
Methanocaldococcus jannaschii	+ (308)	+ (469)	−	+	+
Methanococcus maripaludis	+ (309)	+ (468)	−	+	+
Methanopyrus kandleri	−	+ (459)	−	+	+
Methanosarcina mazei	+ (350)	−	+	−	+
Methanosarcina barkeri	+ (356)	−	+	−	+
Methanosarcina acetivorans	+ (350)	−	+	−	+
Methanococcoides burtonii	+ (345)	−	+	−	+
Thermoplasma acidophilum	+ (304)	−	−	−	−
Archaeoglobus fulgidus	−	−	−	+	+

Fig. 8 The phylogenetic distribution of MM1309 orthologues is unrelated to those of the pyrrolysine, selenocysteine, and phosphoserine systems. A plus or minus sign indicates whether the genes encoding MM1309-like proteins, aSelB, PylRS, SelD, and SepRS, exist in archaea. The numbers of amino acid residues (a.a.) in the MM1309-like proteins and aSelBs are also shown

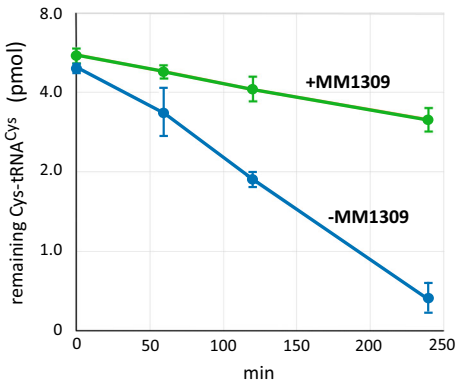

Fig. 9 MM1309 binds Cys-tRNA^{Cys} and slows its hydrolysis. The reaction mixture was prepared without MM1309 and Cys-tRNA^{Cys}, and then Cys-tRNA^{Cys} or Cys-tRNA^{Cys} preincubated with MM1309 was added to each tube. The reactions were stopped at after 0, 1, 2, and 4 h by adding 10 % trichloroacetic acid (TCA), and were washed several times with TCA. Then, the radioactivities were measured with a liquid scintillation counter. The *vertical axis* is plotted on a logarithmic scale. Cys-tRNA^{Cys} in the presence of MM1309 (*green line*) exhibited slower deacylation than that without MM1309 (*blue line*). The half-lives of Cys-tRNA^{Cys} with and without MM1309 were about 300 and 80 min, respectively. *Error bars* SD (n = 3)

Materials and methods

Materials, enzymes, and chemicals

Biochemical and molecular biological procedures were performed using commercially available enzymes, chemicals, and other materials. GTP, GDP, and guanosine 5′-(β,γ-imido)triphosphate (GMPPNP) were purchased from Sigma-Aldrich (USA). [2′-/3′-*O*-(*N*-methylanthraniloyl)guanosine-5′-*O*-triphosphate] (Mant-GTP) and [2′-/3′-*O*-(*N*-methylanthraniloyl)guanosine-5′-*O*-diphosphate] (Mant-GDP) were purchased from Jena Bioscience (Germany). [α-^{32}P]GTP (800 Ci/mmol) and [^{14}C] L-cystine (74 GBq/mmol) were purchased from Perkin Elmer (USA).

Cloning, expression, and purification of *M. mazei* MM1309

The *M. mazei* MM1309 gene was cloned into the pET28c vector (Novagen). The native and selenomethionine (SeMet)-substituted proteins were overexpressed in *E. coli* BL21(DE3) and B834(DE3) cells, respectively. The cell pellet was resuspended and sonicated in 50 mM potassium phosphate buffer (pH 7.4), containing 10 mM imidazole, 500 mM NaCl, 5 mM β-mercaptoethanol, 10 % glycerol, and protease inhibitor cocktail (Complete-EDTA free, Roche) (buffer A). After centrifugation, the supernatant was loaded on a HisTrap column (GE Healthcare), and the protein was eluted with buffer A containing 500 mM imidazole, instead of 10 mM imidazole. Fractions containing the MM1309 protein were pooled and dialyzed against 50 mM potassium phosphate buffer (pH 7.4), containing 50 mM NaCl, 1 mM DTT, 10 % glycerol, and protease inhibitor cocktail (buffer B). The dialyzed fraction was then loaded on a Resource Q column (GE Healthcare), and the flow-through fraction was applied to a hydroxyapatite column (BioRad). After washing the column with buffer B, the bound proteins were eluted by a linear gradient of 0.05–0.83 M NaCl. The proteins were dialyzed against buffer B, and then loaded onto a HiTrap heparin column (GE Healthcare). After washing the column with buffer B, the proteins were eluted by a linear gradient of 0.05–0.83 M NaCl. Prior to crystallization, the MM1309 protein fraction was dialyzed against 10 mM Tris–HCl buffer (pH 8.0), containing 150 mM NaCl, 10 mM $MgCl_2$, and 10 mM β-mercaptoethanol, and concentrated to 12.1–15.3 mg/ml using an Amicon 15 filter (Millipore).

Crystallization

The MM1309 protein was crystallized by the hanging-drop vapor-diffusion method, at 20 °C. The initial screening of crystallization conditions was conducted using commercially available screening kits. The crystals used for data collection were obtained by mixing 1 μl of protein solution with 1 μl of reservoir solution. The reservoir solution contained 0.1 M sodium acetate buffer (pH 4.4–4.8) and 1.4 M sodium citrate. Plate-shaped crystals grew to dimensions of 0.2 mm × 0.1 mm × 0.04 mm in a day. To obtain the co-crystals of MM1309 with GMPPNP or GDP, the MM1309 protein was crystallized in the presence of 5 mM nucleotide in the crystallization drop. The co-crystals were harvested with a solution containing 5 mM GMPPNP or GDP.

Data collection, structure determination, and refinement

The single-wavelength anomalous dispersion (SAD) data sets from the SeMet derivative protein co-crystals with GMPPNP or GDP were collected at beamline BL5A of the Photon Factory (Tsukuba, Japan). The data set of the native protein was collected at beamline BL41XU of SPring-8 (Harima, Japan). All data were processed using the HKL2000 program suite [83]. The MM1309 crystals belong to the orthorhombic space group $P2_12_12$, with unit cell dimensions of $a = 62.06$, $b = 108.7$, $c = 58.32$ Å, and the asymmetric unit contains one MM1309 molecule. The selenium sites were identified using SnB [84] with the SeMet/GMPPNP data set. The selenium sites were refined and the initial phases were calculated with SOLVE [85]. The phases were improved with density modification, using RESOLVE [85]. The initial model was automatically built by RESOLVE and ArpWarp [86], and was manually refined using O [87], CueMol [http://cuemol.sourceforge.ge.jp/en], and Coot [88]. The atomic model was refined using CNS [89], REFMAC5 [90], and PHENIX [91]. The models showed good stereochemistry and geometry, as analyzed by the programs Procheck [46] and Molprobity [http://molprobity.biochem.duke.edu/, 47]. The structures of the GDP-bound and apo forms were solved by the molecular replacement method, using Molrep [46] with the GMPPNP-bound form model as the search model, and refined in the same manner as the GMPPNP-bound form. Graphical images were prepared with the program PyMOL [http://pymol.sourceforge.net/]. All data collection and refinement statistics are summarized in Table 1. Superimpositions of the Cα traces of the MM1309 structures were produced by the program secondary structure matching (SSM) [92].

Isothermal titration calorimetry (ITC)

ITC experiments were performed with the VP-ITC and auto auto-iTC200 systems (MicroCal, USA). In the calorimeter cell, 25–50 μM MM1309, in 10 mM Tris–HCl buffer (pH 7.5) containing 150 mM NaCl, 5 mM $MgCl_2$, and 10 mM β-mercaptoethanol, was titrated with 1 mM GTP, 0.5 mM GDP, or 1 mM GMPPNP at 25 °C. Aliquots (2–5 μl) of ligands were injected into the 0.4–2-ml cell containing the MM1309 solution, to achieve a complete binding isotherm. The resulting titration curves were fitted using the MicroCal Origin software. The binding constant (K_b), the binding stoichiometry (N), and the enthalpy variations (ΔH) were determined by a nonlinear regression fitting procedure.

Preparation of Cys-tRNA^{Cys}

The *M. mazei* tRNA^{Cys} (5′-GCCAAGGUGGCGGAGCG GUCACGCAAUCGCCAGCAGAGCGAUUCAGUCCUG GUUCAAAUCCGGACCUUGGCUCCA-3′) transcript was prepared by in vitro transcription, according to the standard protocol [93]. Briefly, the transcription reaction was performed at 37 °C for 4 h, in a reaction mixture (5 ml) containing 80 mM Hepes–NaOH buffer (pH 8.1), 20 mM $MgCl_2$, 40 mM KCl, 20 mM dithiothreitol (DTT), 2 mM spermine, 14 μg/ml bovine serum albumin (BSA), 20 mM GMP, 5 mM each of ATP, GTP, CTP and UTP, 0.28 mg/ml T7 RNA polymerase, 5 unit pyrophosphatase (Sigma), 0.5 μl ribonuclease inhibitor (TOYOBO), and 10 μg/ml PCR-amplified DNA as a template. The products were purified by Resource Q column chromatography. The tRNA^{Cys} transcript used in this study was charged with cysteine using *M. mazei* CysRS [58]. The *M. mazei* CysRS gene was amplified from genomic DNA, and cloned into the pET28 vector. *M. mazei* CysRS was overexpressed in *E. coli* BL21-Gold(DE3) (Agilent Technologies), and purified by two column chromatography steps (HisTrap and Resource Q). The CysRS fractions were dialyzed against 20 mM potassium phosphate buffer (pH 7.4), containing 0.15 M NaCl and 5 mM β-ME. The aminoacylation reaction was performed at 37 °C for 20 min, in a reaction mixture containing 40 mM Tris–HCl buffer (pH 7.5), 20 mM $MgCl_2$, 40 mM KCl, 4 mM ATP, 50 mM DTT, 40 μM [^{14}C]-L-cystine (74 GBq/mmol), 5 μM *M. mazei* CysRS, and 10 μM *M. mazei* tRNA^{Cys}. The Cys-tRNA^{Cys} was purified by ethanol precipitation, and finally dissolved in 6 mM potassium acetate (pH 5.0) to a concentration of 2 μM. The concentration of Cys-tRNA^{Cys} was estimated from the labeled amino acids incorporated within the tRNA.

Deacylation assay

The assay was basically performed as previously described [59]. Briefly, the deacylation reaction mixture contained 50 mM Tris–HCl buffer (pH 8.5), 20 mM KCl, 25 mM

NaCl, 7 mM $MgCl_2$, 1 mM DTT, 1 mM GTP, and 4.5 μM Cys-$tRNA^{Cys}$, with or without 33 μM MM1309. The Cys-$tRNA^{Cys}$ was preincubated with or without MM1309 at 30 °C for 10 min, and then the deacylation assay buffer was added. The deacylation reaction was performed at 25 °C for 4 h.

Data deposition

The atomic coordinates and structure factors for the apo form of MM1309, and the GMPPNP- and GDP-bound forms of SeMet-substituted MM1309 from *M. mazei*, have been deposited in the Protein Data Bank (PDB codes: 3WND, 3WNB, and 3WNC, respectively).

Acknowledgments We would like to thank the staff of the beamline BL41XU at SPring-8 (Harima, Japan), as well as the staff of the BL-5A and AR-NW12 beamlines at the Photon Factory (Tsukuba, Japan). We also thank Dr. Takuhiro Ito (The University of Tokyo) for assisting with the data collection, as well as for helpful discussions. We thank Dr. Tomomi Sumida (RIKEN) for technical assistance. We are grateful to Dr. Hirofumi Nakagawa (The University of Tokyo), and Drs. Takuma Kasai and Takashi Umehara (RIKEN) for ITC analyses. We would like to thank Azusa Ishii, Takako Imada, Kojiro Ake, and Tomoko Nakayama for clerical assistance. This work was supported in part by Grants-in-Aid for Scientific Research from the Ministry of Education, Culture, Sports, Science and Technology (MEXT) of Japan, and the RIKEN Structural Genomics/Proteomics Initiative (RSGI) in the National Project on Protein Structural and Functional Analyses, MEXT, and the Targeted Proteins Research Program (TPRP), MEXT.

References

1. Kaziro Y, Itoh H, Kozasa T, Nakafuku M, Satoh T (1991) Structure and function of signal-transducing GTP-binding proteins. Annu Rev Biochem 60:349–400
2. Weijland A, Harmark K, Cool RH, Anborgh PH, Parmeggiani A (1992) Elongation factor Tu: a molecular switch in protein biosynthesis. Mol Microbiol 6:683–688
3. Sprinzl M (1994) Elongation factor Tu: a regulatory GTPase with an integrated effector. Trends Biochem Sci 19:245–250
4. Clark BF, Nyborg J (1997) The ternary complex of EF-Tu and its role in protein biosynthesis. Curr Opin Struct Biol 7:110–116
5. Rodnina MV, Wintermeyer W (2001) Fidelity of aminoacyl-tRNA selection on the ribosome: kinetic and structural mechanisms. Annu Rev Biochem 70:415–435
6. Nilsson J, Nissen P (2005) Elongation factors on the ribosome. Curr Opin Struct Biol 15:349–354
7. Asahara H, Uhlenbeck OC (2005) Predicting the binding affinities of misacylated tRNAs for *Thermus thermophilus* EF-Tu-GTP. Biochemistry 44:11254–11261
8. Rodnina MV, Fricke R, Wintermeyer W (1994) Transient conformational states of aminoacyl-tRNA during ribosome binding catalyzed by elongation factor Tu. Biochemistry 33:12267–12275
9. Ohta S, Nakanishi M, Tsuboi M, Arai K, Kaziro Y (1977) Structural fluctuation of the polypeptide-chain elongation factor Tu. A comparison of factors from *Escherichia coli* and *Thermus thermophilus* HB8. Eur J Biochem 78:599–608
10. Kjeldgaard M, Nissen P, Thirup S, Nyborg J (1993) The crystal structure of elongation factor EF-Tu from *Thermus aquaticus* in the GTP conformation. Structure 1:35–50
11. Berchtold H, Reshetnikova L, Reiser CO, Schirmer NK, Sprinzl M, Hilgenfeld R (1993) Crystal structure of active elongation factor Tu reveals major domain rearrangements. Nature 365:126–132
12. Yatime L, Mechulam Y, Blanquet S, Schmitt E (2006) Structural switch of the gamma subunit in an archaeal aIF2 alpha gamma heterodimer. Structure 14:119–128
13. Schmitt E, Panvert M, Lazennec-Schurdevin C, Coureux PD, Perez J, Thompson A, Mechulam Y (2012) Structure of the ternary initiation complex aIF2-GDPNP-methionylated initiator tRNA. Nat Struct Mol Biol 19:450–454
14. Stolboushkina E, Nikonov S, Zelinskaya N, Arkhipova V, Nikulin A, Garber M, Nikonov O (2013) Crystal structure of the archaeal translation initiation factor 2 in complex with a GTP analogue and Met-$tRNA^{f(Met)}$. J Mol Biol 425:989–998
15. Commans S, Böck A (1999) Selenocysteine inserting tRNAs: an overview. FEMS Microbiol Rev 23:335–351
16. Thanbichler M, Böck A (2001) Functional analysis of prokaryotic SELB proteins. BioFactors 14:53–59
17. Leibundgut M, Flick C, Thanbichler M, Böck A, Ban N (2005) Selenocysteine tRNA-specific elongation factor SelB is a structural chimaera of elongation and initiation factors. EMBO J 24:11–22
18. Berry MJ, Banu L, Harney JW, Larsen PR (1993) Functional characterization of the eukaryotic SECIS elements which direct selenocysteine insertion at UGA codons. EMBO J 12:3315–3322
19. Suppmann S, Persson BC, Böck A (1999) Dynamics and efficiency in vivo of UGA-directed selenocysteine insertion at the ribosome. EMBO J 18:2284–2293
20. Copeland PR, Driscoll DM (1999) Purification, redox sensitivity, and RNA binding properties of SECIS-binding protein 2, a protein involved in selenoprotein biosynthesis. J Biol Chem 274:25447–25454
21. Copeland PR, Fletcher JE, Carlson BA, Hatfield DL, Driscoll DM (2000) A novel RNA binding protein, SBP2, is required for the translation of mammalian selenoprotein mRNAs. EMBO J 19:306–314
22. Srinivasan G, James CM, Krzycki JA (2002) Pyrrolysine encoded by UAG in Archaea: charging of a UAG-decoding specialized tRNA. Science 296:1459–1462
23. Hao B, Gong W, Ferguson TK, James CM, Krzycki JA, Chan MK (2002) A new UAG-encoded residue in the structure of a methanogen methyltransferase. Science 296:1462–1466
24. Krzycki JA (2005) The direct genetic encoding of pyrrolysine. Curr Opin Microbiol 8:706–712
25. Blight SK, Larue RC, Mahapatra A, Longstaff DG, Chang E, Zhao G, Kang PT, Green-Church KB, Chan MK, Krzycki JA (2004) Direct charging of tRNA(CUA) with pyrrolysine in vitro and *in vivo*. Nature 431:333–335
26. Polycarpo C, Ambrogelly A, Berube A, Winbush SM, McCloskey JA, Crain PF, Wood JL, Söll D (2004) An aminoacyl-tRNA synthetase that specifically activates pyrrolysine. Proc Nat Acad Sci USA 101:12450–12454
27. Namy O, Rousset JP, Napthine S, Brierley I (2004) Reprogrammed genetic decoding in cellular gene expression. Mol Cell 13:157–168
28. Ibba M, Söll D (2004) Aminoacyl-tRNAs: setting the limits of the genetic code. Genes Dev 18:731–738
29. Zhang Y, Baranov PV, Atkins JF, Gladyshev VN (2005) Pyrrolysine and selenocysteine use dissimilar decoding strategies. J Biol Chem 280:20740–20751

30. Longstaff DG, Blight SK, Zhang L, Green-Church KB, Krzycki JA (2007) *In vivo* contextual requirements for UAG translation as pyrrolysine. Mol Microbiol 63:229–241
31. Nissen P, Kjeldgaard M, Thirup S, Polekhina G, Reshetnikova L, Clark BF, Nyborg J (1995) Crystal structure of the ternary complex of Phe-tRNA^{Phe}, EF-Tu, and a GTP analog. Science 270:1464–1472
32. Abel K, Yoder MD, Hilgenfeld R, Jurnak F (1996) An alpha to beta conformational switch in EF-Tu. Structure 4:1153–1159
33. Nissen P, Kjeldgaard M, Thirup S, Nyborg J (1999) The crystal structure of Cys-tRNA^{Cys}-EF-Tu-GDPNP reveals general and specific features in the ternary complex and in tRNA. Structure 7:143–156
34. Morikawa K, la Cour TF, Nyborg J, Rasmussen KM, Miller DL, Clark BF (1978) High resolution X-ray crystallographic analysis of a modified form of the elongation factor Tu: guanosine diphosphate complex. J Mol Biol 125:325–338
35. Polekhina G, Thirup S, Kjeldgaard M, Nissen P, Lippmann C, Nyborg J (1996) Helix unwinding in the effector region of elongation factor EF-Tu-GDP. Structure 4:1141–1151
36. Song H, Parsons MR, Rowsell S, Leonard G, Phillips SE (1999) Crystal structure of intact elongation factor EF-Tu from *Escherichia coli* in GDP conformation at 2.05-Å resolution. J Mol Biol 285:1245–1256
37. Schmitt E, Blanquet S, Mechulam Y (2002) The large subunit of initiation factor aIF2 is a close structural homologue of elongation factors. EMBO J 21:1821–1832
38. Roll-Mecak A, Alone P, Cao C, Dever TE, Burley SK (2004) X-ray structure of translation initiation factor eIF2gamma: implications for tRNA and eIF2alpha binding. J Biol Chem 279:10634–10642
39. Sokabe M, Yao M, Sakai N, Toya S, Tanaka I (2006) Structure of archaeal translational initiation factor 2 betagamma-GDP reveals significant conformational change of the beta-subunit and switch 1 region. Proc Natl Acad Sci USA 103:13016–13021
40. Yatime L, Mechulam Y, Blanquet S, Schmitt E (2007) Structure of an archaeal heterotrimeric initiation factor 2 reveals a nucleotide state between the GTP and the GDP states. Proc Natl Acad Sci USA 104:18445–18450
41. Nikonov O, Stolboushkina E, Nikulin A, Hasenöhrl D, Bläsi U, Manstein DJ, Fedorov R, Garber M, Nikonov S (2007) New insights into the interactions of the translation initiation factor 2 from archaea with guanine nucleotides and initiator tRNA. J Mol Biol 373:328–336
42. Milburn MV, Tong L, deVos AM, Brünger A, Yamaizumi Z, Nishimura S, Kim SH (1990) Molecular switch for signal transduction: structural differences between active and inactive forms of protooncogenic ras proteins. Science 247:939–945
43. Sprang SR (1997) G protein mechanisms: insights from structural analysis. Annu Rev Biochem 66:639–678
44. Deppenmeier U, Johann A, Hartsch T, Merkl R, Schmitz RA, Martinez-Arias R, Henne A, Wiezer A, Baeumer S, Jacobi C, Brueggemann H, Lienard T, Christmann A, Boemecke M, Steckel S, Bhattacharyya A, Lykidis A, Overbeek R, Gottschalk G (2002) The genome of *Methanosarcina mazei*: evidence for lateral gene transfer between bacteria and archaea. J Mol Microbiol Biotechnol 4:453–461
45. Atkinson GC, Hauryliuk V, Tenson T (2011) An ancient family of SelB elongation factor-like proteins with a broad but disjunct distribution across archaea. BMC Evol Biol 11:22
46. Collaborative Computational Project (1994) Number 4. Acta Crystallogr. D50:760–763
47. Davis IW, Murray LW, Richardson JS, Richardson DC (2004) MOLPROBITY: structure validation and all-atom contact analysis for nucleic acids and their complexes. Nucleic Acids Res 32:W615–W619
48. Holm L, Kaariainen S, Rosenstrom P, Schenkel A (2008) Searching protein structure databases with DaliLite v. 3. Bioinformatics 24:2780–2781
49. Kobayashi K, Kikuno I, Kuroha K, Saito K, Ito K, Ishitani R, Inada T, Nureki O (2010) Structural basis for mRNA surveillance by archaeal Pelota and GTP-bound EF1α complex. Proc Natl Acad Sci USA 107:17575–17579
50. Kobayashi K, Saito K, Ishitani R, Ito K, Nureki O (2012) Structural basis for translation termination by archaeal RF1 and GTP-bound EF1α complex. Nucleic Acids Res 40:9319–9328
51. Grøftehauge MK, Therkelsen MØ, Taaning R, Skrydstrup T, Morth JP, Nissen P (2013) Identifying ligand-binding hot spots in proteins using brominated fragments. Acta Crystallogr F69:1060–1065
52. Parmeggiani A, Krab IM, Watanabe T, Nielsen RC, Dahlberg C, Nyborg J, Nissen P (2006) Enacyloxin IIa pinpoints a binding pocket of elongation factor Tu for development of novel antibiotics. J Biol Chem 281:2893–2900
53. Holbrook SR, Kim SH (1989) Molecular model of the G protein alpha subunit based on the crystal structure of the HRAS protein. Proc Natl Acad Sci USA 86:1751–1755
54. Saraste M, Sibbald PR, Wittinghofer A (1990) The P-loop-a common motif in ATP- and GTP-binding proteins. Trends Biochem Sci 15:430–434
55. Leipe DD, Wolf YI, Koonin EV, Aravind L (2002) Classification and evolution of P-loop GTPases and related ATPases. J Mol Biol 317:41–72
56. Daviter T, Wieden HJ, Rodnina MV (2003) Essential role of histidine 84 in elongation factor Tu for the chemical step of GTP hydrolysis on the ribosome. J Mol Biol 332:689–699
57. Laalami S, Grentzmann G, Bremaud L, Cenatiempo Y (1996) Messenger RNA translation in prokaryotes: GTPase centers associated with translational factors. Biochimie 78:577–589
58. Mansilla F, Knudsen CR, Laurberg M, Clark BF (1997) Mutational analysis of *Escherichia coli* elongation factor Tu in search of a role for the N-terminal region. Protein Eng 10:927–934
59. Thanbichler M, Böck A, Goody RS (2000) Kinetics of the interaction of translation factor SelB from *Escherichia coli* with guanosine nucleotides and selenocysteine insertion sequence RNA. J Biol Chem 275:20458–20466
60. Arai N, Kaziro Y (1975) Mechanism of the ribosome-dependent uncoupled GTPase reaction catalyzed by polypeptide chain elongation factor G. J Biochem 77:439–447
61. Agrawal RK, Penczek P, Grassucci RA, Frank J (1998) Visualization of elongation factor G on the *Escherichia coli* 70S ribosome: the mechanism of translocation. Proc Natl Acad Sci USA 95:6134–6138
62. Agrawal RK, Heagle AB, Penczek P, Grassucci RA, Frank J (1999) EF-G-dependent GTP hydrolysis induces translocation accompanied by large conformational changes in the 70S ribosome. Nat Struct Biol 6:643–647
63. Stark H, Rodnina MV, Wieden HJ, van Heel M, Wintermeyer W (2000) Large-scale movement of elongation factor G and extensive conformational change of the ribosome during translocation. Cell 100:301–309
64. Valle M, Zavialov A, Sengupta J, Rawat U, Ehrenberg M, Frank J (2003) Locking and unlocking of ribosomal motions. Cell 114:123–134
65. Hansson S, Singh R, Gudkov AT, Liljas A, Logan DT (2005) Crystal structure of a mutant elongation factor G trapped with a GTP analogue. FEBS Lett 579:4492–4497
66. Wilden B, Savelsbergh A, Rodnina MV, Wintermeyer W (2006) Role and timing of GTP binding and hydrolysis during EF-G-dependent tRNA translocation on the ribosome. Proc Natl Acad Sci USA 103:13670–13675
67. Connell SR, Takemoto C, Wilson DN, Wang H, Murayama K, Terada T, Shirouzu M, Rost M, Schüler M, Giesebrecht J,

Dabrowski M, Mielke T, Fucini P, Yokoyama S, Spahn CM (2007) Structural basis for interaction of the ribosome with the switch regions of GTP-bound elongation factors. Mol Cell 25:751–764
68. Hauryliuk V, Hansson S, Ehrenberg M (2008) Cofactor dependent conformational switching of GTPases. Biophys J 95:1704–1715
69. Noble CG, Song H (2008) Structural studies of elongation and release factors. Cell Mol Life Sci 65:1335–1346
70. Frolova L, Le Goff X, Zhouravleva G, Davydova E, Philippe M, Kisselev L (1996) Eukaryotic polypeptide chain release factor eRF3 is an eRF1- and ribosome-dependent guanosine triphosphatase. RNA 2:334–341
71. Kong C, Ito K, Walsh MA, Wada M, Liu Y, Kumar S, Barford D, Nakamura Y, Song H (2004) Crystal structure and functional analysis of the eukaryotic class II release factor eRF3 from *S. pombe*. Mol Cell 14:233–245
72. Hauryliuk V, Zavialov A, Kisselev L, Ehrenberg M (2006) Class-1 release factor eRF1 promotes GTP binding by class-2 release factor eRF3. Biochimie 88:747–757
73. des Georges A, Hashem Y, Unbehaun A, Grassucci RA, Taylor D, Hellen CU, Pestova TV, Frank J (2014) Structure of the mammalian ribosomal pre-termination complex associated with eRF1-eRF3-GDPNP. Nucleic Acids Res 42:3409–3418
74. Zavialov AV, Buckingham RH, Ehrenberg M (2001) A posttermination ribosomal complex is the guanine nucleotide exchange factor for peptide release factor RF3. Cell 107:115–124
75. Gao H, Zhou Z, Rawat U, Huang C, Bouakaz L, Wang C, Cheng Z, Liu Y, Zavialov A, Gursky R, Sanyal S, Ehrenberg M, Frank J, Song H (2007) RF3 induces ribosomal conformational changes responsible for dissociation of class I release factors. Cell 129:929–941
76. Zhou J, Lancaster L, Trakhanov S, Noller HF (2012) Crystal structure of release factor RF3 trapped in the GTP state on a rotated conformation of the ribosome. RNA 18:230–240
77. Roll-Mecak A, Cao C, Dever TE, Burley SK (2000) X-ray structures of the universal translation initiation factor IF2/eIF5B: conformational changes on GDP and GTP binding. Cell 103:781–792
78. Roll-Mecak A, Alone P, Cao C, Dever TE, Burley SK (2003) X-ray structure of translation initiation factor eIF2 gamma: implications for tRNA and eIF2alpha binding. J Biol Chem 279:10634–10642
79. Kuhle B, Ficner R (2014) eIF5B employs a novel domain release mechanism to catalyze ribosomal subunit joining. EMBO J 33:1177–1191
80. Paleskava A, Konevega AL, Rodnina MV (2012) Thermodynamics of the GTP-GDP-operated conformational switch of selenocysteine-specific translation factor SelB. J Biol Chem 287:27906–27912
81. Hauenstein SI, Perona JJ (2008) Redundant synthesis of cysteinyl-tRNA^{Cys} in *Methanosarcina mazei*. J Biol Chem 283:22007–22017
82. Pingoud A, Urbanke C, Krauss G, Peters F, Maass G (1977) Ternary complex formation between elongation factor Tu, GTP and aminoacyl-tRNA: an equilibrium study. Eur J Biochem 78:403–409
83. Otwinowski Z, Minor W (1997) Processing of X-ray Diffraction Data Collected in Oscillation Mode. Methods Enzymol 276:307–326
84. Weeks CM, Miller R (1999) Optimizing Shake-and-Bake for proteins. Acta Crystallogr. D55:492–500
85. Terwilliger TC (2003) SOLVE and RESOLVE: automated structure solution and density modification. Methods Enzymol 374:22–37
86. Cohen SX, Ben Jelloul M, Long F, Vagin A, Knipscheer P, Lebbink J, Sixma TK, Lamzin VS, Murshudov GN, Perrakis A (2008) ARP/wARP and molecular replacement: the next generation. Acta Crystallogr D64:49–60
87. Jones TA, Zou JY, Cowan SW, Kjeldgaard M (1991) Improved methods for building protein models in electron density maps and the location of errors in these models. Acta Crystallogr A47:110–119
88. Emsley P, Cowtan K (2004) Coot: model-building tools for molecular graphics. Acta Crystallogr D60:2126–2132
89. Brünger AT, Adams PD, Clore GM, DeLano WL, Gros P, Grosse-Kunstleve RW, Jiang JS, Kuszewski J, Nilges M, Pannu NS, Read RJ, Rice LM, Simonson T, Warren GL (1998) Simulated-annealing real-space refinement as a tool in model building. Acta Crystallogr D54:905–921
90. Murshudov GN, Skubák P, Lebedev AA, Pannu NS, Steiner RA, Nicholls RA, Winn MD, Long F, Vagin AA (2011) REFMAC5 for the refinement of macromolecular crystal structures. Acta Crystallogr D67:355–367
91. Adams PD, Afonine PV, Bunkóczi G, Chen VB, Davis IW, Echols N, Headd JJ, Hung L-W, Kapral GJ, Grosse-Kunstleve RW, McCoy AJ, Moriarty NW, Oeffner R, Read RJ, Richardson DC, Richardson JS, Terwilliger TC, Zwart PH (2010) PHENIX: a comprehensive Python-based system for macromolecular structure solution. Acta Crystallogr D66:213–221
92. Krissinel E, Henrick K (2004) Secondary-structure matching (SSM), a new tool for fast protein structure alignment in three dimensions. Acta Crystallogr D60:2256–2268
93. Yanagisawa T, Ishii R, Fukunaga R, Kobayashi T, Sakamoto K, Yokoyama S (2008) Crystallographic studies on multiple conformational states of active-site loops in pyrrolysyl-tRNA synthetase. J Mol Biol 378:634–652
94. Thompson JD, Higgins DG, Gibson TJ (1994) CLUSTAL W: improving the sensitivity of progressive multiple sequence alignment through sequence weighting, position-specific gap penalties and weight matrix choice. Nucleic Acids Res 22:4673–4680
95. Gouet P, Courcelle E, Stuart DI, Metoz F (1999) ESPript: analysis of multiple sequence alignments in PostScript. Bioinformatics 15:305–308